

Article

Homogeneous Nucleation Mechanism of NaCl in Aqueous Solutions

Qiang Sun *, Shuai Cui and Meixi Zhang

Key Laboratory of Orogenic Belts and Crustal Evolution, Ministry of Education, The School of Earth and Space Sciences, Peking University, Beijing 100871, China; 1801210217@pku.edu.cn (S.C.); mx-zhang@pku.edu.cn (M.Z.)

* Correspondence: QiangSun@pku.edu.cn

Received: 17 January 2020; Accepted: 10 February 2020; Published: 12 February 2020



Abstract: In this study, molecular dynamic simulations are employed to investigate the homogeneous nucleation mechanism of NaCl crystal in solutions. According to the simulations, the dissolved behaviors of NaCl in water are dependent on ion concentrations. With increasing NaCl concentrations, the dissolved Na^+ and Cl^- ions tend to be aggregated in solutions. In combination with our recent studies, the aggregate of dissolved solutes is mainly ascribed to the hydrophobic interactions. Different from the two-step mechanism, no barrier is needed to overcome the formation of the aggregate. In comparison with the classical nucleation theory (CNT), because of the formation of solute aggregate, this lowers the barrier height of nucleation and affects the nucleation mechanism of NaCl crystal in water.

Keywords: nucleation; CNT; water; hydrophobic interactions; aggregate

1. Introduction

The nucleation of crystals in liquids is one of the most ubiquitous phenomena in nature. It is crucial in geology and environmental sciences, where the formation and behavior of crystalline solids may change with temperature, pressure, and chemical environment. In addition, nucleation plays an important role in many practical applications, ranging from semiconductors, metals, chemicals, to pharmaceuticals. Therefore, many experimental and theoretical works have been devoted to investigate the nucleation mechanism in aqueous solutions.

Generally, nucleation is described by the classical nucleation theory (CNT). CNT is based on the assumption that the free energy necessary to create a nucleus of n particles can be divided into a favorable term, proportional to the number of particles in the nucleus, and an unfavorable term, proportional to the dividing surface between the nucleus and the solution. The free energy difference can be analytically expressed as,

$$\Delta G_{CNT} = -\Delta\mu \cdot n + \gamma \cdot s \quad (1)$$

where $\Delta\mu$ is the difference in chemical potential between the crystal and the liquid phase, n is the number of molecules in the crystal phase, γ is the surface tension, and s is the surface of the nucleus. Therefore, the critical nucleus (N_c) can be expected in CNT.

Recently, many experimental approaches [1–13] have been employed to investigate the thermodynamics and kinetics of crystal nucleation in liquids, such as optical microscopy, atomic force microscopy, cryo-TEM, ultrafast X-ray scattering, et al. These lead to the confirmation of the presence of the intermediate phase, such as amorphous calcium carbonate (ACC) [3,4], which are relevant to the solidification pathway of the dissolved solutes. Therefore, a two-step mechanism of nucleation of crystals in solution was put forth [14–16]. In the first step, amorphous nuclei are formed—their surface energy is lower than that of crystalline nuclei as a consequence of their disordered interfaces with the

solution. In the second step, an amorphous-to-crystalline transition takes place in the middle of the amorphous phase. Compared with direct crystallization from solution, this transition overcomes a much lower free energy barrier.

In addition, many works [17–25] have also been conducted to investigate the nucleation mechanism of NaCl from the solutions. Zahn [17] found that ion aggregates were particularly stable when a Na^+ ion was octahedrally coordinated by Cl^- ions. In Giberti et al. study [18], they employed metadynamics simulations to find an intriguing wurtzite-like polymorph, which was suggested to be an intermediate route from brine to the final rock salt structure. According to Chakraborty and Patey study [23], this means that a dense but unstructured NaCl nucleus is first formed, and rearranged into the rock salt structure. Therefore, this is in agreement with a two-step mechanism. In recent Jiang et al. [24] work, they identify a transition from one- to two-step crystallization mechanism driven by a spinodal. In addition, some works [26,27] were conducted on the nucleation mechanism of KCl in water. In Peng et al. study [26], this indicates that there are high density KCl ionic clusters prior to nucleation.

Nucleation processes are classed as homogeneous and heterogeneous [28]. In fact, nucleation in liquids occurs heterogeneously more often than not [29,30]. In heterogeneous nucleation, the surface of some different substance acts as the centre upon which the first atoms, ions, or molecules of the crystal become properly oriented. Heterogeneous nucleation can customarily be formulated within the CNT framework, which is related to homogeneous nucleation through the shape factor changing from 0 to 1 [31]. Therefore, it is important to investigate the mechanism of homogeneous nucleation. In this study, molecular dynamic simulations are employed to investigate the homogeneous nucleation mechanism of NaCl crystal in solutions.

2. Molecular Dynamics Simulations

2.1. Simulated Systems

Molecular dynamics (MD) simulations were conducted using the GROMACS (version 5.14) [32,33]. The simulated results were analyzed through Plumed (version 2.4) [34,35]. At 298 K and 0.1 MPa, the NaCl solubility (Mass Fraction, w) in water is 26.483% [36]. To investigate the nucleation mechanism of NaCl crystal in solutions, MD simulations are conducted on slightly oversaturated NaCl solutions ($\text{NaCl}:\text{H}_2\text{O} = 223:2000$). In principle, the nucleation mechanism was closely related to the dissolved behaviors of NaCl in water. To investigate the structure of NaCl solutions, MD simulations were also conducted on various NaCl- H_2O systems (Table 1).

Table 1. The simulated systems in this work.

No.	System	NaCl	H_2O	(Mass Fraction, 100w)
1	NaCl- H_2O	1	2000	0.16
2	NaCl- H_2O	2	2000	0.32
3	NaCl- H_2O	3	2000	0.48
4	NaCl- H_2O	4	2000	0.65
5	NaCl- H_2O	5	2000	0.81
6	NaCl- H_2O	10	2000	1.60
7	NaCl- H_2O	20	2000	3.15
8	NaCl- H_2O	30	2000	4.64
9	NaCl- H_2O	40	2000	6.10
10	NaCl- H_2O	50	2000	7.51
11	NaCl- H_2O	223	2000	26.58

The SPC/E model was used for water, and the ion parameters were those used in the OPLS force field. These force fields have been widely applied to investigate the homogeneous nucleation of NaCl [21,23] and KCl [27] crystals in water. The simulations were carried out in the NPT ensemble. The simulated temperature was kept at 300 K, employing Nose-Hoover thermostat dynamics. The pressure was maintained at 1 atm using a Parrinello-Rahman pressure coupling. The simulated box was initially kept at $42 \text{ \AA} \times 42 \text{ \AA} \times 42 \text{ \AA}$, and NaCl salts were uniformly embedded in the box. Additionally, periodic boundary conditions were applied in all three directions. The Lennard-Jones interactions were truncated at 1.0 nm. The particle mesh Ewald method was used to calculate the long range electrostatics forces. Additionally, each simulation time was 60000 ps with a time step of 2 fs.

2.2. Order Parameters

Generally, the Steinhardt parameters [37] were applied to measure the degree of order in the system. In this work, both local Q4 (LOCAL Q4) and local Q6 parameters (LOCAL Q6) were calculated to measure the degree of order during the nucleation of NaCl in the solutions, which were based on the corresponding fourth (q4) and sixth (q6) order Steinhardt parameters. Regarding the sixth order Steinhardt parameters, it measured the degree to which the first coordination shell around an atom was ordered. With reference to atom i , the Steinhardt parameter was calculated as,

$$q_{6m}(i) = \frac{\sum_j \sigma(r_{ij}) Y_{6m}(r_{ij})}{\sum_j \sigma(r_{ij})} \quad (2)$$

where Y_{6m} was one of the sixth order spherical harmonics so m was a number that runs from -6 to $+6$. The function $\sigma(r_{ij})$ was a switching function that acted on the distance between atoms i and j . Additionally, for LOCAL Q6 parameter, it measured the extent to which the orientation of the atoms in the first coordination sphere of an atom matched the orientation of the central atom. It was determined as,

$$s_i = \frac{\sum_j \sigma(r_{ij}) \sum_{m=-6}^6 q_{6m}^*(i) q_{6m}(j)}{\sum_j \sigma(r_{ij})} \quad (3)$$

where $q_{6m}(i)$ and $q_{6m}(j)$ were the sixth order Steinhardt vectors calculated for atom i and atom j , and the asterisk denoted complex conjugation.

2.3. Metadynamics

To investigate the nucleation mechanism from the solutions, the changes of free energy was reconstructed through Metadynamics method of Laio and Parrinello [38,39]. Metadynamics belonged to the family of enhanced sampling techniques in which the probability of visiting high free energy states was increased by adding to the Hamiltonian an adaptive external potential. The external repulsive potential was typically written as a series of Gaussian functions that were deposited in the space of collective variables (CVs) as,

$$V(S, t) = \sum_{kT < t} W(kT) \exp \left(- \sum_{i=1}^d \frac{(s_i - s_i^{(0)}(kT))^2}{2\sigma_i^2} \right) \quad (4)$$

where W and σ were the height and the width of the added Gaussians, respectively. Because of the external potentials, the system could freely diffuse above the potential energy surface, completely sampling the CVs space. At this point, the free energy surface (FES) as a function of the set of CVs was obtained as the negative of the repulsive bias deposited during the course of the simulation,

$$V(s) = -F(s) \quad (5)$$

3. Discussions

3.1. The Structure of NaCl Solutions

The NaCl RDFs have a first contact maximum at 2.8 Å (CIP, contact ion pairs), second solvent-separated maximum at 5.1 Å (SSIP, solvent separated ion pairs), and a weak third maximum at about 7 Å corresponding to an attraction of fully hydrated ions. For dilute NaCl solutions (NaCl:H₂O = 1:2000), the RDFs are dominated by SSIP states (Figure 1). With increasing salt concentrations, this leads to a rise of the first maximum and a fall of the second in the Na-Cl RDFs (Figure 1). This is in correspondence with other studies on the structure of NaCl solutions [40,41]. Additionally, the structural changes can also be observed in the experimental measurements of aqueous LiCl solutions [42–44].

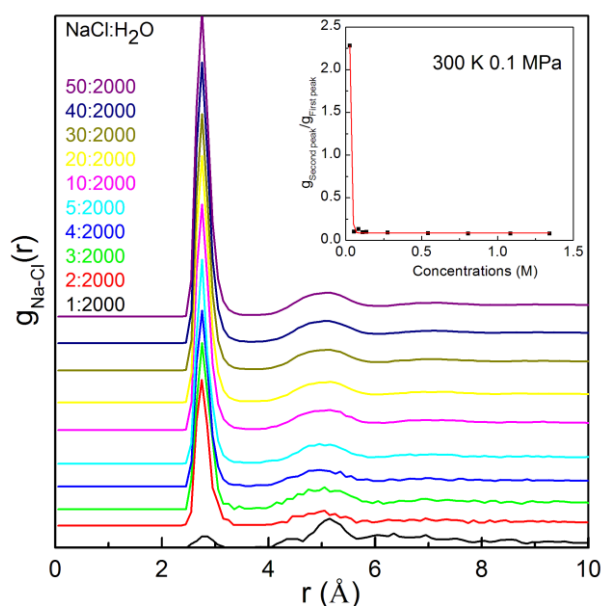


Figure 1. The calculated $g_{\text{Na-Cl}}(r)$ of various NaCl solutions. The inset shows the dependence of the ratio of second peak to the first peak of $g_{\text{Na-Cl}}(r)$ on the NaCl concentrations.

In principle, radial distribution function $g_{ij}(r)$, where $r = |r_i - r_j|$ stands for the separation between a particle of component i and of component j , gives the probability of finding two particles at some distance r , taking account of density and geometric effects. This is related to the potential of mean force (PMF) between two particles, and can be expressed as,

$$W_{\text{PMF}(r)} = -k_B T \ln g(r) \quad (6)$$

Therefore, the changes of $g_{ij}(r)$ indicate that the PMF of the separation between the particles is dependent on the NaCl concentrations.

For dilute NaCl solutions, the Na-Cl RDFs are dominated by SSIP. This means that the ions prefer to SSIP in dilute NaCl concentrations, and SSIP is thermodynamically stable than CIP. It is contrast with the PMF between a Na⁺ and a Cl[−] ions in water [45], which shows that the first minimum (CIP at 2.8 Å) is lower than the second minimum (SSIP at 5.1 Å). Therefore, this indicates that the CIP and SSIP configurations may be separated by a high (several kT) effective potential barrier and transitions between them are rare events. In other words, it seems that there exists “repulsive” force between the dissolved ions in dilute NaCl solutions. Therefore, it is necessary to study the structure of water, and the effects of dissolved NaCl on water structure.

Many works have been devoted to investigate the structure of liquid water, which can roughly be partitioned into two categories: (a) mixture models and (b) continuum models [46]. Based on

Raman spectroscopic studies on water structure [47–49], when three-dimensional hydrogen-bonded networks appear, various OH vibrational frequencies correspond to different hydrogen-bonded networks in the first shell of a water molecule (local hydrogen bonding). This indicates that OH vibrations are mainly dependent on the local hydrogen bonding of a water molecule, and the effects of hydrogen bonding beyond the first shell on OH vibrations are weak. Therefore, for ambient water, a water molecule interacts with neighboring water molecules (in the first shell) through various local hydrogen-bonded networks.

When NaCl salts are dissolved in water, they dissociate into ions that are hydrated. Because of the interactions between dissolved ions and water molecules around the ions, the dissolved ions affect the structure of hydrated water molecules, which may be different from that in bulk water. The structure and dynamics of water around ions have been studied with neutron and X-ray diffraction [41,50], X-ray absorption spectroscopy [51], femtosecond time-resolved infrared (fs-IR) vibrational spectroscopy [52–54], and optical Kerr-effect spectroscopy [55], respectively. These reports support the notion that the effect of ions on water is largely limited to the first solvation shell. In fact, this is in agreement with the above discussion on the dependence of OH vibrations on water structure. The OH vibrations are dependent on local hydrogen bondings, therefore the dissolved ions mainly affect the structure of water molecules within their first coordination shell.

In principle, when solutes are dissolved into water, the thermodynamic functions may contain solute–solute, solute–water, and water–water interaction energies, respectively.

$$\Delta G = \Delta G_{\text{Water-water}} + \Delta G_{\text{Solute-water}} + \Delta G_{\text{Solute-solute}} \quad (7)$$

In our Raman spectroscopic studies on NaCl solutions [48], as NaCl is dissolved into water, this mainly lowers the sub-band around 3220 cm^{-1} , and raises the sub-band around 3430 cm^{-1} . Therefore, the dissolved NaCl breaks the hydrogen bondings of water, and the hydrogen bonding strength of NaCl-water is weaker than that of water-water. Therefore, the “repulsive” force between the Na^+ and Cl^- ions in dilute NaCl solutions may be closely related to hydrogen bonding of water, which results in the ions to be occupied by SSIP configurations.

From the simulations, with increasing NaCl concentrations, the dissolved ions tend to form CIP rather than SSIP. Additionally, as NaCl salts increases, these decrease the separations between Cl^- and Cl^- ions, and between Na^+ and Na^+ ions, especially $g_{\text{Cl-Cl}(r)}$ (Figure 2). This is in agreement with the experimental studies on the structure of NaCl and LiCl solutions [40–44]. Therefore, with increasing NaCl concentrations, the dissolved Na^+ and Cl^- ions tend to be aggregated. This is in agreement with other molecular dynamics simulations [56] and experimental studies [57,58] on NaCl solutions.

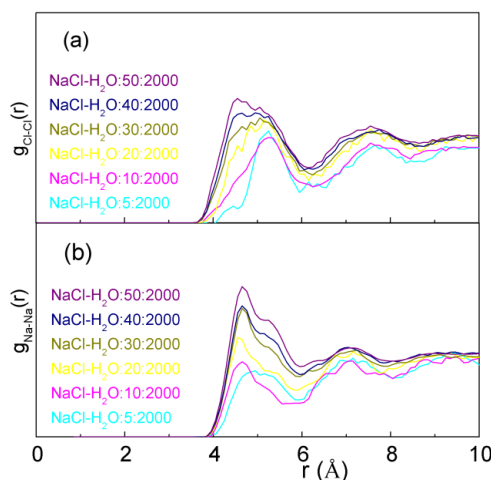


Figure 2. The calculated $g_{\text{Cl-Cl}(r)}$ (a) and $g_{\text{Na-Na}(r)}$ (b) functions of NaCl solutions.

In addition, the ion aggregation can also be demonstrated by the dependence of hydrogen bondings on NaCl concentrations (Figure 3). In this study, the geometrical definition of hydrogen bonding is utilized to determine the hydrogen bonds in water [59]. If r_{OO} and $\angle OOH$ are less than 3.5 \AA and 30° , a hydrogen bonding is considered to exist between two water molecules. As NaCl is dissolved into water, this decreases the hydrogen bondings in water. However, with increasing NaCl concentrations, the effects of NaCl salts on hydrogen bondings become weak. This is due to the dissolved ions are aggregated in water, which decreases the surface area of ions available for water molecules.

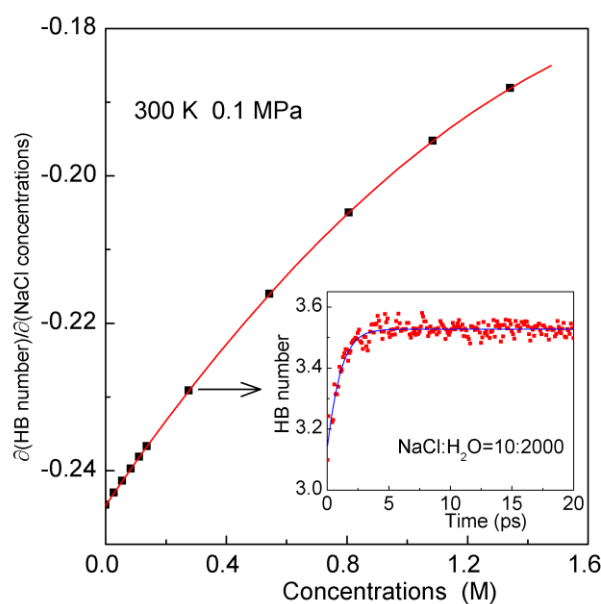


Figure 3. The effects of NaCl salts on hydrogen bonding in water. The fitted line is shown in solid. The inset shows the changes of hydrogen bonding of NaCl solutions (NaCl:H₂O = 10:2000) as the system approaching the equilibrium.

In this study, the ion aggregated distribution in solutions is termed as the aggregate. Similar concepts are also used to reflect the aggregation, such as amorphous calcium carbonate (ACC) or pre-nucleation clusters (PNC) [3–6]. According to the calculated $g_{\text{Na-Cl}}(r)$, the ion is regarded to be engaged into the aggregate as the separation between the Na^+ and Cl^- being less than the first minimum (3.5 \AA). With increasing NaCl concentrations, this increases the number of ion aggregate (Figure 4).

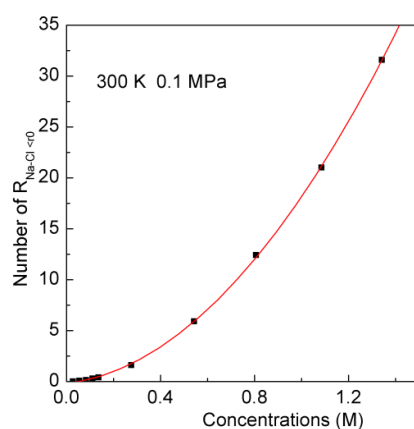


Figure 4. The number of $g_{\text{Na-Cl}}(r)$ less than the first minimum (3.5 \AA) in various NaCl solutions. The fitted line is shown in solid.

In fact, the solute aggregates have been reported in many experimental methods [1–13], such as transmission electron microscopy (TEM), atomic force microscopy (AFM), small angle X-ray scattering and light scattering. They are described to be short-range order and long-range disorder, and formed via aggregation of solution species comprised of ion complexes or multi-ion clusters, and may exist in equilibrium with the free monomers. The aggregate is observed not only for organic and colloidal systems but also for various electrolyte solutions. It is important to investigate the origin of solute aggregate in solutions.

In the recent work by Marcus [60], the average distance apart of the centers of the ions in a c M solution of a symmetrical electrolyte is $d(\text{nm}) = 0.94 [c/M]$. Therefore, if the dissolved ions are homogeneously distributed in water, ion pairing can be expected at highly concentrated (>1 M) solutions. However, besides the highly concentrated solutions, there is now much evidence indicating that ion aggregate can be found in lower concentrations (<1 M) [61,62]. Therefore, it is necessary to investigate the driving force of solute aggregation in aqueous solutions.

The classic Debye-Hückel theory [63], valid only for dilute electrolytes, predicts that the interaction between two charged surfaces in an electrolyte decays exponentially with the surface separation [64] with a decay length, called the Debye length. In fact, the screening length characterizes the range over which the perturbation due to an electrical double layer extends. The screening length is about 10 nm in dilute ~ 1 mM solutions, it decreases to 0.8 nm in ~ 150 mM solutions. In general, it can be expected that the high ion density would result in a short-range screening of an external electric field. However, based on the surface force measurements, it decays exponentially with the separation between sheets, beyond a short-range layering regime, namely “underscreening” in concentrated electrolyte solutions [65–67]. From Israelachvili et al. [68] surface force measurements, it means a decay length of the force, about 10–13 nm.

In dilute solutions, if the dissolved ions are dominated by the electrostatic interactions between them, the CIP can be expected rather than SSIP. This is in contrast with the experimental and theoretical studies [40,41], which mean that the dissolved ions prefer to SSIP in dilute solutions. This indicates that, as slats are dissolved into water, the cation–anion attraction in the crystal may be overwhelmed by favorable ion–water interactions. Therefore, the dissolved behaviors of ions may be closely related to the hydrogen bondings of water. In addition, regarding to “underscreening,” it is based on the measurements of the force between two interfaces separated by a thin aqueous, which show the increase in decay length with increasing salt concentration at high salt concentrations. In combination with the above discussion, it can be derived that the attraction between the interfaces may be related to the hydrogen bondings of water.

To investigate the changes of hydrogen bonding of water in the formation of ion aggregate, the hydrogen bonding number is calculated. In this study, the NaCl solutions are initially setup where the Na^+ and Cl^- ions are homogeneously distributed in water. As the simulated system approaching the equilibrated state where the ions are aggregated, this is accompanied with the increase of hydrogen bonding in water (Figure 3 inlet). Because the strength of water–water hydrogen bonding is stronger than that of NaCl–water interactions, the driving force of ion aggregation can reasonably be ascribed to maximize the hydrogen bonding in water, which affects the global distributions of dissolved ions. Additionally, the local distributions may be affected by electrostatic force between the ions.

According to recent studies on water structure [47–49] and air/water interface [69], the hydration free energy is derived, which is utilized to investigate the physical origin of hydrophobic effects. It can be found that hydrophobic effects are ascribed to the structural competition between hydrogen bondings in bulk water and those in interfacial water [70–72]. With increasing solute concentrations, it can be divided into initial and hydrophobic solvation processes, which correspond to various dissolved behaviors of solutes, such as dispersed and accumulated distributions in water. This is in agreement with the simulations on NaCl solutions.

In general, hydrophobic effects are described as the tendency of non-polar molecules or molecular surfaces to aggregate in an aqueous solution. From our recent study on the physical origin on

hydrophobic effects [70], it is attributed to the strength of hydrogen bonding of bulk water is stronger than that of interfacial water. In fact, hydrophobic effects may be extended to other systems only if the strength of solute/solvent interface is weaker than that of bulk solvent. Therefore, hydrophobic interactions can be applied to understand the dissolved behaviors of NaCl salts in water.

As the foreign substances, such as solid particles, are embedded into water, the interfaces appear between the particles and water. They mainly affect the structure of interfacial water (the topmost water layer at the interface), which undoubtedly affect the dissolved behaviors of solutes. To maximize the hydrogen bondings of bulk water, the dissolved solutes tend to be aggregated at the surface of the substances. Therefore, because of the existence of the foreign substances in the solutions, it is helpful to form the solute aggregate at the foreign surfaces.

From this work, with increasing NaCl concentrations, the dissolved Na^+ and Cl^- ions tend to be aggregated in water. It should be noted that the tendency of ion aggregation may be counterbalanced by thermal motions. Additionally, based on our recent study on hydrophobic effects [70], it can be derived that the hydrophobic interactions of ion aggregate may be inversely proportional to the size of ion aggregate. Therefore, as the size of ion aggregate increases, the strength of hydrophobic interactions also increases.

3.2. NaCl Nucleation

In this study, MD simulations are conducted on slightly oversaturated NaCl solutions to investigate the nucleation of NaCl crystal in water. Based on the calculated Na-Cl RDFs, these can be applied to study the nucleation process of NaCl in the solutions. Compared with the Na-Cl RDFs prior to the nucleation, the second peak is well split as NaCl crystal appears in the solutions (Figure 5). As NaCl crystals grow, both the third and fourth peaks can be detected in the RDFs. Additionally, the nucleation can be found to first take place in the solute aggregate of the solutions. This is in accordance with other experimental and theoretical studies on the nucleation mechanism [15,16].

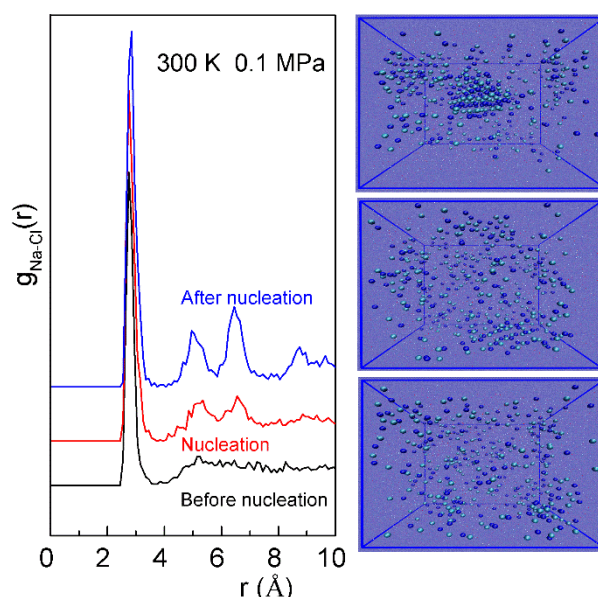


Figure 5. The $g_{\text{Na-Cl}}(r)$ of NaCl solutions ($\text{NaCl}:\text{H}_2\text{O} = 223:2000$) in the process of nucleation. The corresponding configurations are also shown (from bottom to top).

In some works, this nucleation is explained through Ostwald's Law of Stages or Ostwald's Rule [73]. It means that, when several solid phases exist, the formation of the thermodynamically stable phase can be preceded by metastable intermediates that stepwise transform to the final product. Namely that, in the case of a compound capable of crystallizing in several forms, it will be the least

stable form, which is first produced by the spontaneous crystallization, followed successively by the forms of increasing stability. However, the aggregate is found in not only oversaturated but also non-saturated solutions, the structure can be described as the short-range order and long-range disorder. Therefore, it is unreasonable to understand the aggregate through Ostwald's rule.

Different from the aggregate, the structure of crystal is characterized by the periodic lattice of elementary unit. In this work, both LQ4 and LQ6 parameters are calculated and utilized to distinguish the NaCl crystals in the aqueous solutions. As the NaCl crystal nucleates from the solutions, this increases the order parameter of LQ4 and LQ6 (Figure 6). This is also in correspondence with the changes of Na-Cl RDFs. Therefore, both LQ4 and LQ6 can be applied to measure the nucleation process of NaCl crystal in the solutions.

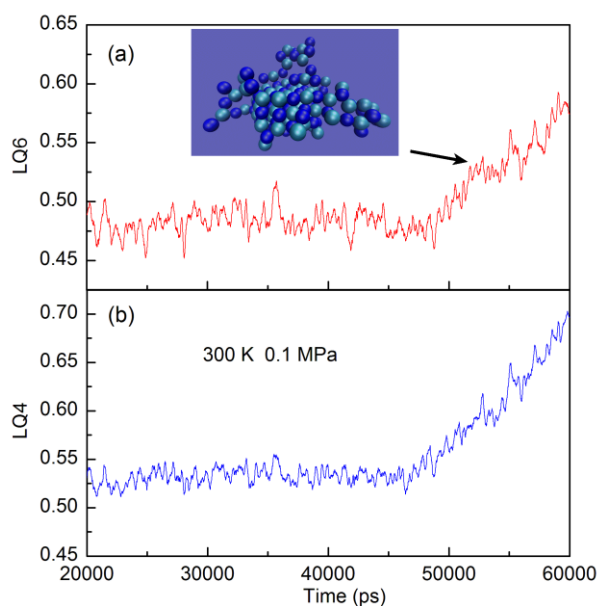


Figure 6. The changes of local Q6 (a) and Q4 (b) parameter of NaCl solutions (NaCl:H₂O = 223:2000) during the nucleation. As the nucleation of NaCl crystal occurs, the max aggregate of NaCl (Agg_c) is shown (The ion number is 169).

To investigate the changes of free energy in the process of NaCl nucleation, based on LQ4 and LQ6 parameters, the free energy surface (FES) can be determined through the METAD method (Figure 7). It can be found that only one potential barrier is necessary to overcome so that the nucleation of NaCl crystal proceeds. Based on the calculated LQ4 and LQ6 of the solutions, the lowest zone of FES is in correspondence with the formation of ion aggregate in the solutions. Therefore, no barrier is necessary to overcome in the formation of the aggregate. Because of the ion aggregation, this makes the system to be more thermodynamically stable. In other words, the dissolved ions tend to be aggregated in the solutions.

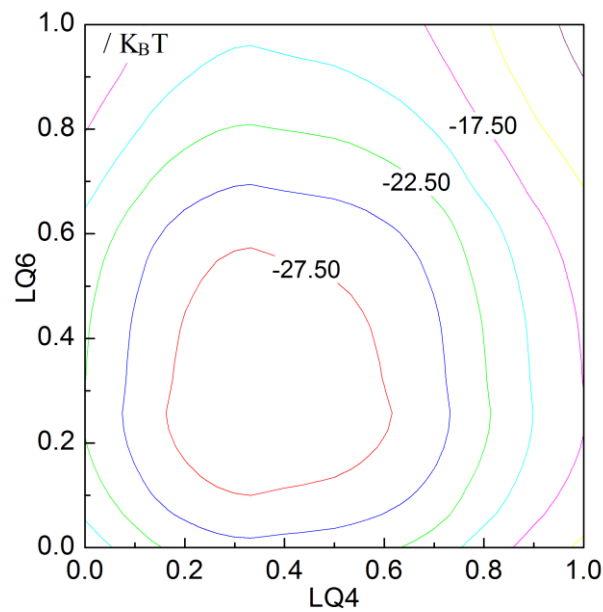


Figure 7. The free energy surface (FES) as the function of LQ4 and LQ6 in the nucleation process of NaCl crystal in the solutions (NaCl:H₂O = 223:2000).

From the simulations, the nucleation of NaCl crystal first takes place in the ion aggregate. This indicates that, because of the formation of ion aggregate, it is helpful for forming NaCl crystal in the solutions. In other words, the ion aggregate may correspond to the nucleation site with the relatively lower height of nucleation barrier. In combination with the above discussion, it can be derived that, because of the hydrophobic interactions, this leads to the formation of solute aggregate, and also lowers the height of nucleation barrier.

Based on this study, it can be found that the formation of the ion aggregate is not considered in CNT theory. To understand the nucleation mechanism from aqueous solutions, it is necessary to take into account the hydrophobic interactions. Because the ion aggregation lowers the height of potential barrier, the CNT can reasonably be revised as (Rev-CNT),

$$\Delta G_{\text{Rev}} = \Delta G_{\text{CNT}} - \Delta G_H \quad (8)$$

where ΔG_H means the hydrophobic interactions in the formation of ion aggregate. Different from the critical nuclei of CNT, the critical aggregate (Agg_C) can be expected, which corresponds to the largest aggregate as the nucleation occurs in water.

In combination with our recent studies on hydrophobic interaction [70–72], the ΔG_H is the difference of Gibbs energy as the solutes are transformed from dispersed to accumulated distributions in water. In this work, the solute is treated as a hydrophobic sphere. After the aggregate is regarded as an ideal sphere, the ΔG_H is expressed as,

$$\Delta G_H = 8 \cdot \frac{(n - n^{-\frac{1}{3}})}{r} \cdot \Delta G_{\text{DDAA}} \cdot r_{\text{H}_2\text{O}} \quad \left(R = n^{\frac{1}{3}} \cdot r \right) \quad (9)$$

where ΔG_{DDAA} is the Gibbs energy of DDAA (tetrahedral) hydrogen bonding, $r_{\text{H}_2\text{O}}$ is the radius of a H₂O molecule, r is the radius of solute, R is the size of solute aggregate, and n is the solute number of aggregate. From this, it can be derived that the larger the solute number of aggregate (or aggregate size), the stronger the hydrophobic interactions. Therefore, the nucleation is expected to take place in the largest aggregate, and the Agg_C corresponds to the largest aggregate as nucleation occurs in solutions.

From this work, the nucleation of NaCl crystal can be described as the ion dispersed distribution → the ion aggregate → the nucleation (Figure 8). For the driving force of ion aggregate, it

is due to maximize the hydrogen bonding of water. Regarding to the origin of solute aggregate, it is closely related to hydrophobic interactions. Different from two-step nucleation, no barrier is necessary to overcome to form the aggregate. Therefore, only one barrier is needed to overcome in the process of nucleation. In comparison with CNT, because of the formation of solute aggregate, this lowers the height of potential barrier of nucleation, and affects the nucleation mechanism of NaCl in water.

Regarding the CNT theory, it does not take into account the effects of hydrophobic interactions on the dissolved behaviors of solutes in water. Therefore, CNT may be applied to investigate the nucleation as hydrophobic interactions can be ignored. In combination with this study, this means that CNT can be utilized to understand the nucleation mechanism as the solutes are dispersed in solutions (Figure 8).

As the foreign substances are embedded into water, they mainly affect the structure of interfacial water. From the above, to maximize the hydrogen bondings of bulk water, the dissolved solutes tend to be aggregated at the surface of the substances. Because of the existence of the foreign surfaces, it is helpful to form the solute aggregate. Additionally, this reduces the height of the nucleation barrier, thereby facilitating the phase transition (heterogeneous nucleation). In combination with recent studies [74], it can be found that heterogeneous nucleation may be closely related to the geometric characteristics of foreign surface, especially geometric shape. Additionally, it may be also affected by the molecular polarity of the substance surface. Further study is necessary.

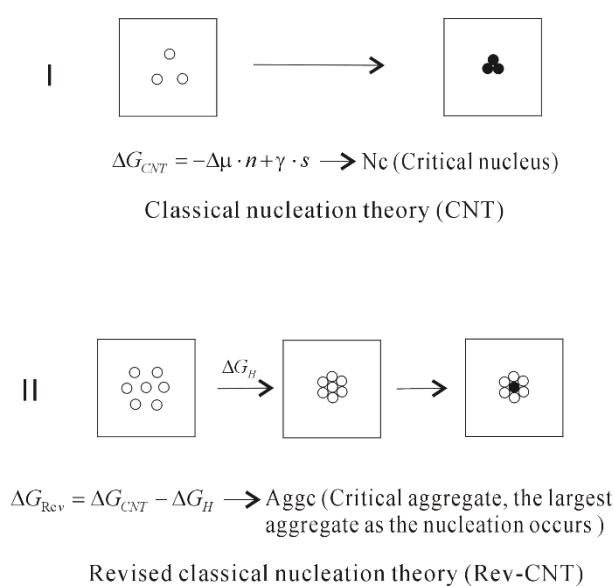


Figure 8. The homogeneous nucleation mechanism of dissolved solutes in water. The dissolved behaviors of NaCl in water are dependent on ion concentrations, which affect the nucleation mechanism of NaCl crystal in water. Because of the formation of solute aggregate, this reduces the height of nucleation barrier.

4. Conclusions

In this work, molecular dynamic simulations are applied to investigate the nucleation mechanism of NaCl in solutions. From this study, the following conclusions can be derived,

- (1) According to the simulations, the dissolved behaviors of NaCl in water are dependent on ion concentrations. With increasing NaCl concentrations, the dissolved behaviors of Na^+ and Cl^- ions are transformed from dispersed to aggregated distributions in water.
- (2) In combination with our recent studies on hydrophobic interactions, the solute aggregate is mainly ascribed to the hydrophobic interactions. Thermodynamically, no barrier is needed to overcome in the formation of the solute aggregate.

- (3) In comparison with the CNT, because of the formation of ion aggregate in solutions, this lowers the barrier height of nucleation, and affects the nucleation mechanism (Rev-CNT). Therefore, the nucleation of crystal can be expected to take place in the largest aggregate (Agg_C).

Author Contributions: Q.S. designed the research; Q.S. performed simulations; Q.S. analyzed the data; Q.S. wrote the paper; Q.S., S.C., and M.Z. revised the paper. All authors have read and agreed to the published version of the manuscript.

Funding: This work is supported by the National Natural Science Foundation of China (Grant Nos. 41773050).

Conflicts of Interest: The authors declare no conflict of interest.

References

1. Bøjesen, E.D.; Iversen, B.B. The chemistry of nucleation. *CrystEngComm* **2016**, *18*, 8332–8353. [[CrossRef](#)]
2. DeYoreo, J.J. In-situ liquid phase TEM observations of nucleation and growth processes. *Prog. Cryst. Growth Charact. Mater.* **2016**, *62*, 69–88. [[CrossRef](#)]
3. Khouzani, M.F.; Chevrier, D.M.; Güttlein, P.; Hauser, K.; Zhang, P.; Hedinc, N.; Gebauer, D. Disordered amorphous calcium carbonate from direct precipitation. *CrystEngComm* **2015**, *17*, 4842–4849. [[CrossRef](#)]
4. Pouget, E.M.; Bomans, P.H.H.; Goos, J.A.C.M.; Frederik, P.M.; de With, G.; Sommerdijk, N.A.J.M. The initial stages of template-controlled CaCO₃ formation revealed by cryo-TEM. *Science* **2009**, *323*, 1455–1458. [[CrossRef](#)]
5. Gebauer, D.; Colfen, H. Prenucleation clusters and non-classical nucleation. *Nano Today* **2011**, *6*, 564–584. [[CrossRef](#)]
6. Gebauer, D.; Kellermeier, M.; Gale, J.D.; Bergstrom, L.; Colfen, H. Pre-nucleation clusters as solute precursors in crystallization. *Chem. Soc. Rev.* **2014**, *43*, 2348–2371. [[CrossRef](#)]
7. Nielsen, M.H.; Aloni, S.; De Yoreo, J.J. In situ TEM imaging of CaCO₃ nucleation reveals coexistence of direct and indirect pathways. *Science* **2014**, *345*, 1158–1162. [[CrossRef](#)]
8. Kellermeier, M.; Picker, A.; Kempter, A.; Cölfen, H.; Gebauer, D. A straightforward treatment of activity in aqueous CaCO₃ solutions and the consequences for nucleation theory. *Adv. Mater.* **2014**, *26*, 752–757. [[CrossRef](#)]
9. Gebauer, D.; Völkel, A.; Cölfen, H. Stable prenucleation calcium carbonate clusters. *Science* **2008**, *322*, 1819–1822. [[CrossRef](#)]
10. Zhang, T.H.; Liu, X.Y. Nucleation: What happens at the initial stage? *Angew. Chem. Int. Ed.* **2009**, *48*, 1308–1312. [[CrossRef](#)]
11. Smeets, P.J.M.; Cho, K.R.; Kempen, R.G.E.; Sommerdijk, N.A.J.M.; De Yoreo, J.J. Calcium carbonate nucleation driven by ion binding in a biomimetic matrix revealed by in situ electron microscopy. *Nat. Mater.* **2015**, *14*, 394–399. [[CrossRef](#)] [[PubMed](#)]
12. Lupulescu, A.I.; Rimer, J.D. In situ imaging of silicalite-1 surface growth reveals the mechanism of crystallization. *Science* **2014**, *344*, 729–732. [[CrossRef](#)] [[PubMed](#)]
13. Loh, N.D.; Sen, S.; Bosman, M.; Tan, S.F.; Zhong, J.; Nijhuis, C.A.; Král, P.; Matsudaira, P.; Mirsaidov, U. Multistep nucleation of nanocrystals in aqueous solution. *Nat. Chem.* **2017**, *9*, 77–82. [[CrossRef](#)]
14. ten Wolde, P.R.; Frenkel, D. Enhancement of protein crystal nucleation by critical density fluctuations. *Science* **1997**, *277*, 1975–1978. [[CrossRef](#)] [[PubMed](#)]
15. Vekilov, P.G. The two-step mechanism of nucleation of crystals in solution. *Nanoscale* **2010**, *2*, 2346–2357. [[CrossRef](#)] [[PubMed](#)]
16. Karthika, S.; Radhakrishnan, T.K.; Kalaichelvi, P. A review of classical and nonclassical nucleation theories. *Cryst. Growth Des.* **2016**, *16*, 6663–6681. [[CrossRef](#)]
17. Zahn, D. Atomistic mechanism of NaCl nucleation from an aqueous solution. *Phys. Rev. Lett.* **2004**, *92*, 040801. [[CrossRef](#)]
18. Giberti, F.; Tribello, G.A.; Parrinello, M. Transient polymorphism in NaCl. *J. Chem. Theory Comput.* **2013**, *9*, 2526–2530. [[CrossRef](#)]
19. Zimmermann, N.E.R.; Vorselaars, B.; Quigley, D.; Peters, B. Nucleation of NaCl from aqueous solution: Critical sizes, ion-attachment kinetics, and rates. *J. Am. Chem. Soc.* **2015**, *137*, 13352–13361. [[CrossRef](#)]

20. Alejandre, J.; Hansen, J.P. Ions in water: From ion clustering to crystal nucleation. *Phys. Rev. E* **2007**, *76*, 061505. [[CrossRef](#)]
21. Chakraborty, D.; Patey, G.N. How crystals nucleate and grow in aqueous NaCl solution. *J. Phys. Chem. Lett.* **2013**, *4*, 573–578. [[CrossRef](#)] [[PubMed](#)]
22. Lanaro, G.; Patey, G.N. Birth of NaCl crystals: Insights from molecular simulations. *J. Phys. Chem. B* **2016**, *120*, 9076–9087. [[CrossRef](#)]
23. Chakraborty, D.; Patey, G.N. Evidence that crystal nucleation in aqueous NaCl solution occurs by the two-step mechanism. *Chem. Phys. Lett.* **2013**, *587*, 25–29. [[CrossRef](#)]
24. Jiang, H.; Debenedetti, P.G.; Panagiotopoulos, A.Z. Nucleation in aqueous NaCl solutions shifts from 1-step to 2-step mechanism on crossing the spinodal. *J. Chem. Phys.* **2019**, *150*, 124502. [[CrossRef](#)] [[PubMed](#)]
25. Patel, L.A.; Kindt, J.T. Simulations of NaCl aggregation from solution: Solvent determines topography of free energy landscape. *J. Comput. Chem.* **2019**, *40*, 135–147. [[CrossRef](#)]
26. Peng, H.; Gudgeon, J.; Vaughan, J. Nucleation phenomena of supersaturated KCl solutions revealing by molecular dynamic simulation: Implication of dehydration shell process. *J. Mol. Liq.* **2019**, *283*, 108–115. [[CrossRef](#)]
27. Ahmadi, S.; Wu, Y.; Rohani, S. Molecular dynamics simulation of homogeneous nucleation of supersaturated potassium chloride (KCl) in aqueous solutions. *CrystEngComm* **2019**, *21*, 7507–7518. [[CrossRef](#)]
28. Sosso, G.C.; Chen, J.; Cox, S.J.; Fitzner, M.; Pedevilla, P.; Zen, A.; Michaelides, A. Crystal nucleation in liquids: Open questions and future challenges in molecular dynamics simulations. *Chem. Rev.* **2016**, *116*, 7078–7116. [[CrossRef](#)]
29. Oshchepkov, M.; Popov, K.; Ryabova, A.; Redchuk, A.; Tkachenko, S.; Dikareva, J.; Koltinova, E. Barite crystallization in presence of novel fluorescent-tagged antiscalants. *Int. J. Corros. Scale Inhib.* **2019**, *8*, 998–1021.
30. Oshchepkov, M.; Kamagurov, S.; Tkachenko, S.; Ryabova, A.; Popov, K. Insight into the mechanisms of scale inhibition: A case study of a task-specific fluorescent-tagged scale inhibitor location on gypsum crystals. *ChemNanoMat* **2019**, *5*, 586–592. [[CrossRef](#)]
31. Kalikmanov, V. *Nucleation Theory*; Springer: Dordrecht, The Netherlands, 2013; Volume 860.
32. Berendsen, H.J.C.; van der Spoel, D.; van Drunen, R. GROMACS: A message-passing parallel molecular dynamics implementation. *Comput. Phys. Commun.* **1995**, *91*, 43–56. [[CrossRef](#)]
33. van der Spoel, D.; Lindahl, E.; Hess, B.; Groenhof, G.; Mark, A.E.; Berendsen, H.J.C. GROMACS: Fast, flexible and free. *J. Comput. Chem.* **2005**, *26*, 1701–1718. [[CrossRef](#)] [[PubMed](#)]
34. Bonomi, M.; Branduardi, D.; Bussi, G.; Camilloni, C.; Provasi, D.; Raiteri, P.; Donadio, D.; Marinelli, F.; Pietrucci, F.; Broglia, R.A.; et al. PLUMED: A portable plugin for free-energy calculations with molecular dynamics. *Phys. Commun.* **2009**, *180*, 1961–1972. [[CrossRef](#)]
35. Tribello, G.A.; Giberti, F.; Sosso, G.C.; Salvalaglio, M.; Parrinello, M. Analyzing and driving cluster formation in atomistic simulations. *J. Chem. Theory Comput.* **2017**, *13*, 1317–1327. [[CrossRef](#)] [[PubMed](#)]
36. Pinho, S.P.; Macedo, E.A. Solubility of NaCl, NaBr, and KCl in water, methanol, ethanol, and their mixed solvents. *J. Chem. Eng. Data* **2005**, *50*, 29–32. [[CrossRef](#)]
37. Steinhardt, P.J.; Nelson, D.R.; Ronchetti, M. Bond-orientational order in liquids and glasses. *Phys. Rev. B* **1983**, *28*, 784–805. [[CrossRef](#)]
38. Laio, A.; Parrinello, M. Escaping free energy minima. *Proc. Natl. Acad. Sci. USA* **2002**, *99*, 12562–12566. [[CrossRef](#)]
39. Laio, A.; Gervasio, F.L. Metadynamics: A method to simulate rare events and reconstruct the free energy in biophysics, chemistry and material science. *Rep. Prog. Phys.* **2008**, *71*, 126601. [[CrossRef](#)]
40. Bouazizi, S.; Nasr, S.; Jaidane, N.; Bellissent-Funel, M.C. Local order in aqueous NaCl solutions and pure water: X-ray scattering and molecular dynamics simulations study. *J. Phys. Chem. B* **2006**, *110*, 23515–23523. [[CrossRef](#)]
41. Mancinelli, R.; Botti, A.; Bruni, F.; Ricci, M.A.; Soper, A.K. Hydration of sodium, potassium, and chloride ions in solution and the concept of structure maker/breaker. *J. Phys. Chem. B* **2007**, *111*, 13570–13577. [[CrossRef](#)]
42. Bouazizi, S.; Nasr, S. Local order in aqueous lithium chloride solutions as studied by X-ray scattering and molecular dynamics simulations. *J. Mol. Struct.* **2007**, *837*, 206–213. [[CrossRef](#)]

43. Bouazizi, S.; Hammami, F.; Nasr, S.; Bellissent-Funel, M.C. Neutron scattering experiments on aqueous sodium chloride solutions and heavy water. Comparison to molecular dynamics and X-ray results. *J. Mol. Struct.* **2008**, *892*, 47–52. [[CrossRef](#)]
44. Bouazizi, S.; Nasr, S. Structural investigations of high concentrated aqueous LiCl solutions: X-ray scattering and MD simulations approach. *J. Mol. Struct.* **2008**, *875*, 121–129. [[CrossRef](#)]
45. Luksic, M.; Fennell, C.J.; Dill, K.A. Using interpolation for fast and accurate calculation of ion-ion interactions. *J. Phys. Chem. B* **2014**, *118*, 8017–8025. [[CrossRef](#)]
46. Stanley, H.E.; Teixeira, J. Interpretation of the unusual behavior of H₂O and D₂O at low temperatures: Tests of a percolation model. *J. Chem. Phys.* **1980**, *73*, 3404–3422. [[CrossRef](#)]
47. Sun, Q. The Raman OH stretching bands of liquid water. *Vib. Spectrosc.* **2009**, *51*, 213–217. [[CrossRef](#)]
48. Sun, Q. Raman spectroscopic study of the effects of dissolved NaCl on water structure. *Vib. Spectrosc.* **2012**, *62*, 110–114. [[CrossRef](#)]
49. Sun, Q. Local statistical interpretation for water structure. *Chem. Phys. Lett.* **2013**, *568*, 90–94. [[CrossRef](#)]
50. Collins, K.D.; Neilson, G.W.; Enderby, J.E. Ions in water: Characterizing the forces that control chemical processes and biological structure. *Biophys. Chem.* **2007**, *128*, 95–104. [[CrossRef](#)]
51. Cappa, C.D.; Smith, J.D.; Messer, B.M.; Cohen, R.C.; Saykally, R.J. Effects of cations on the hydrogen bond network of liquid water: New results from X-ray absorption spectroscopy of liquid microjets. *J. Phys. Chem. B* **2006**, *110*, 5301–5309. [[CrossRef](#)]
52. Omta, A.W.; Kropman, M.F.; Woutersen, S.; Bakker, H.J. Negligible effect of ions on the hydrogen-bond structure in liquid water. *Science* **2003**, *301*, 347–349. [[CrossRef](#)] [[PubMed](#)]
53. Park, S.; Fayer, M.D. Hydrogen bond dynamics in aqueous NaBr solutions. *Proc. Natl. Acad. Sci. USA* **2007**, *104*, 16731–16738. [[CrossRef](#)] [[PubMed](#)]
54. Moilanen, D.E.; Wong, D.; Rosenfeld, D.E.; Fenn, E.E.; Fayer, M.D. Ion-water hydrogen-bond switching observed with 2D IR vibrational echo chemical exchange spectroscopy. *Proc. Natl. Acad. Sci. USA* **2009**, *106*, 375–380. [[CrossRef](#)]
55. Turton, D.A.; Hunger, J.; Hefter, G.; Buchner, R.; Wynne, K. Glasslike behavior in aqueous electrolyte solutions. *J. Chem. Phys.* **2008**, *128*, 161102. [[CrossRef](#)]
56. Chen, A.A.; Pappu, R.V. Quantitative characterization of ion pairing and cluster formation in strong 1:1 electrolytes. *J. Phys. Chem. B* **2007**, *111*, 6469–6478. [[CrossRef](#)]
57. Boerner, B.R.; Bates, R.G. Conductance of HCl, NaCl, Na acetate, and acetic acid in water-ethylene carbonate solvent mixtures at 25 and 40 °C. *J. Sol. Chem.* **1978**, *7*, 245–256. [[CrossRef](#)]
58. De Robertis, A.; Di Giacomo, P.; Foti, C. Ion-selective electrode measurements for the determination of formation constants of alkali and alkaline earth metals with low-molecular-weight ligands. *Anal. Chim. Acta* **1995**, *300*, 45–51. [[CrossRef](#)]
59. Kumar, R.; Schmidt, J.R.; Skinner, J.L. Hydrogen bonding definitions and dynamics in liquid water. *J. Chem. Phys.* **2007**, *126*, 204107. [[CrossRef](#)]
60. Marcus, Y. Effect of ions on the structure of water: Structure making and breaking. *Chem. Rev.* **2009**, *109*, 1346–1370. [[CrossRef](#)]
61. Samal, S.; Geckeler, K.E. Unexpected solute aggregation in water on dilution. *Chem. Commun.* **2001**, *21*, 2224–2225. [[CrossRef](#)]
62. van der Vegt, N.F.A.; Haldrup, K.; Roke, S.; Zheng, J.R.; Lund, M.; Bakker, H.J. Water-mediated ion pairing: Occurrence and relevance. *Chem. Rev.* **2016**, *116*, 7626–7641. [[CrossRef](#)] [[PubMed](#)]
63. Hückel, E.; Debye, P. Zur theorie der elektrolyte. I. Gefrierpunktniedrigung und verwandte erscheinungen. *Physikalische Zeitschrift* **1923**, *24*, 185–206.
64. Israelachvili, J.N. *Intermolecular and Surface Forces*; Academic Press: London, UK, 2011.
65. Gebbie, M.A.; Dobbs, H.A.; Valtiner, M.; Israelachvili, J.N. Long-range electrostatic screening in ionic liquids. *Proc. Natl. Acad. Sci. USA* **2015**, *112*, 7432–7437. [[CrossRef](#)] [[PubMed](#)]
66. Smith, A.M.; Lee, A.A.; Perkin, S. The electrostatic screening length in concentrated electrolytes increases with concentration. *J. Phys. Chem. Lett.* **2016**, *7*, 2157–2163. [[CrossRef](#)]
67. Lee, A.A.; Perez-Martinez, C.S.; Smith, A.M.; Perkin, S. Underscreening in concentrated electrolytes. *Faraday Discuss.* **2017**, *199*, 239–259. [[CrossRef](#)]
68. Gebbie, M.A.; Valtiner, M.; Banquy, X.; Fox, E.T.; Henderson, W.A.; Israelachvili, J.N. Ionic liquids behave as dilute electrolyte solutions. *Proc. Natl. Acad. Sci. USA* **2013**, *110*, 9674–9679. [[CrossRef](#)]

69. Sun, Q.; Guo, Y. Vibrational sum frequency generation spectroscopy of the air/water interface. *J. Mol. Liq.* **2016**, *213*, 28–32. [[CrossRef](#)]
70. Sun, Q. The physical origin of hydrophobic effects. *Chem. Phys. Lett.* **2017**, *672*, 21–25. [[CrossRef](#)]
71. Sun, Q.; Su, X.W.; Cheng, C.B. The dependence of hydrophobic interactions on the solute size. *Chem. Phys.* **2019**, *516*, 199–205. [[CrossRef](#)]
72. Sun, Q.; Zhang, M.X.; Cui, S. The structural origin of hydration repulsive force. *Chem. Phys. Lett.* **2019**, *714*, 30–36. [[CrossRef](#)]
73. Threlfall, T. Structural and thermodynamic explanations of Ostwald’s rule. *Org. Process Res. Dev.* **2003**, *7*, 1017–1027. [[CrossRef](#)]
74. Kiselev, A.; Bachmann, F.; Pedevilla, P.; Cox, S.; Michaelides, A.; Gerthsen, D.; Leisner, T. Active sites in heterogeneous ice nucleation—the example of K-rich feldspars. *Science* **2017**, *355*, 367–371. [[CrossRef](#)] [[PubMed](#)]



© 2020 by the authors. Licensee MDPI, Basel, Switzerland. This article is an open access article distributed under the terms and conditions of the Creative Commons Attribution (CC BY) license (<http://creativecommons.org/licenses/by/4.0/>).